INTERNATIONAL JOURNAL OF COMPUTERS
Issue 4, Volume 2, 2008

Solid Modelling with Fourth Order Partial Differential Equation

L. H. You, P. Comninos, and Jian J. Zhang

***Abstract*—** A solid modeling method is developed in this paper. In order to satisfy the tangential continuity, a fourth order partial differential equation is proposed and the boundary conditions defining the solid are presented. Since an analytical expression of solid models is the fastest in the geometric modeling, a unified closed form solution to the partial differential equation is sought which accurately satisfies the boundary conditions of solids. A number of examples are presented to demonstrate the applications of the developed method in solid modeling and the effects of vector-valued parameters, force function, geometric parameters and basic functions on the shape of solids.

***Keywords*—** Solid modelling, fourth order partial differential equation, closed form solution, shape manipulation.

I. Introduction

Most of the objects that we come across, both in the physical world and in engineering, are best described by their volume. Although the appearance of such objects can be modelled by a surface representation, many applications, such as CAD, metal forming or even simulations of surgical operations, require information pertaining to the entire volume of an object rather than just its surface. Thus, solid or volume modelling is an important aspect of geometric modelling.

Like surface modelling [1-3], volume modelling can be realised by purely geometric methods relying on Bézier, B-spline or NURBS formulations. With such formulations the definition and manipulation of the shape of the solid model are achieved through the placement and movement of a lattice of control points. When the number of these control points becomes large, the task of manipulating the shape of the solid becomes cumbersome. In addition, any physical object that we wish to model may posses a number of physical or mechanical properties that we may also wish to model. Although it is possible to simulate such properties with a purely geometric approach, it is more difficult to do so than with physically-based modelling techniques.

To resolve such problems, physically-based modelling techniques have been developed over the past twenty years, which primarily represent a solid by its surface model. In 1987, Terzopoulos et al. employed the continuous elasticity theory to model the shape and motion of deformable bodies [4]. A year later, Terzopoulos and Fleischer expanded this model to cope with viscoelasticity, plasticity and fracture [5, 6]. Since NURBS have become an industry standard, Terzopoulos and Qin applied the Lagrangian mechanics of an elastic surface and the finite element method to develop dynamic NURBS [7]. Given that many objects exhibit symmetries and topological variability, they introduced dynamic free-form NURBS swung surfaces for modelling this class of objects [8]. In order to overcome the limitations of tensor product NURBS surfaces that are topologically rectangular, they developed dynamic triangular NURBS which are superior as they can be defined over arbitrary parametric domains and produce non-degenerate multi-sided surface patches [9]. Léon and Veron, and Guillet and Léon applied the mechanics of bar networks to deform multi-patch tensor based free-form surfaces [10, 11]. By minimising an energy functional (subject to user controlled geometric constraints and loads), Celniker and Gossard proposed deformable curve and surface finite-elements for free-form shape design [12]. To reduce the computational burden of the finite element method for free-form deformations, Kang and Kak developed a new algorithm that works at two different levels of resolution. Initially, a coarse resolution is used to calculate the overall 3D deformation and, subsequently, a finer resolution is used to deform the surface layers of the object [13]. Work on reducing the computational cost of physically-based modelling was also carried out by Vassilev, who preserved the natural representation of the B-spline surface control points (in a two dimensional array) and presented a more efficient method for manipulating deformable B-spline surfaces by minimising an energy functional [14].

These physically-based modelling techniques, although effective, have to solve a large set of equations that are computationally expensive and not particularly well suited to interactive computer graphics applications.

Surface-modelling techniques based on the solution of partial differential equations have recently become more actively investigated. Rather than manipulating the control points, these modelling techniques modify the surface shape of a solid by adjusting the vector-valued parameters and the force function of the PDE (representing the solid), and / or the positional, tangential and curvature functions of the boundary condition expressions of this equation. In many applications,

Manuscript received April 11, 2008: Revised version received December 16, 2008.

L. H. You, P. Comninos and Jian J. Zhang are with National Centre for Computer Animation, Bournemouth University, Talbot Campus, Poole, BH12 5BB, United Kingdom (e-mail: {lyou|peterc|jzhang}@ Bournemouth.ac.uk).

PDE-based methods are simpler to use and more convenient for the representation of surface models.

Bloor and Wilson were the first to use PDEs to perform surface blending [15] and free-form surface modelling [16]. Most recently, Monterde and Ugail presented a new technique to create surfaces from prescribed boundaries using elliptic partial differential equation operators [17]. Since the solution of fourth order PDEs is the key to the successful generation of PDE surfaces, some numerical methods such as the finite element method [18, 19], the finite difference method [20], and the collocation method [21] were also developed. However, these numerical methods require expensive computation, which hinders their wider application to interactive computer graphics and CAD. In order to overcome this limitation, Bloor and Wilson proposed the spectral method [22] that is efficient for simple boundary conditions but less accurate than other methods.

Since the vector-valued parameters of the PDE have a strong influence on the generated surface shape, You and Zhang have proposed a more general PDE [23] for surface modelling that introduced a larger set of vector-valued parameters. Later, they investigated surface blending using the solution of a fourth order PDE [24] and a sixth order PDE [25]. They also investigated vase design, using a fourth order PDE [26], and surface modelling, using a sixth order PDE [27].

As in the physical world all objects have volume, solid modelling has a wide range of applications in computer graphics and CAD. Due to the complexity of solid modelling, however, only a limited number of publications on physically-based volume modelling have appeared to date.

As early as 1984, Barr developed a set of hierarchical solid modelling operations that simulate twisting, bending, tapering and other similar transformations of geometric objects [28]. In 1992, Requicha and Rossignac conducted a survey of the field of solid modelling and assessed the strengths and weaknesses of the various solid modelling techniques [29]. The same year, Metaxas and Terzopoulos developed a systematic approach to deriving dynamic models from parametrically defined solid primitives, global geometric deformations and local finite-element deformations, and proposed efficient constraint methods for connecting these new dynamic primitives together to construct articulated models [30]. The following year, Bloor and Wilson presented examples of some specific solid volumes generated by solving a second order PDE [31]. In 2000, Ferley et al. presented a sculpture metaphor for rapid shape prototyping that allows the use of free-form shaping tools (which can be designed inside the application) and that can mimic local deformations [32]. The following year, Breen and Whitaker presented an approach to 3D shape metamorphosis that has some advantages over other methods. These advantages include a minimal need for user input, no nodal parameterisation, flexible topology and sub-voxel accuracy [33]. By combining a fourth-order elliptic PDE for the definition of solid volumes with the equation of motion from Dynamics, Du and Qin developed a technique for modelling dynamic solids [34]. In their paper, the finite difference discretization and the multi-grid subdivision techniques were employed to solve numerically the combined equation. In 2002, McDonnell and Qin presented a sculptured solid modelling system, founded upon free-form splines [35]. In 2004, Hua and Qin presented a novel interactive solid modelling framework known as "haptic-based dynamic implicit solid modelling", which is founded upon volumetric implicit functions and powerful physics-based modelling [36]. Developed from PDE-based flow constraints and scalar fields of implicit functions, they also proposed a versatile efficient and intuitive scalar-field-guided adaptive-shape-deformation (SFD) technique for shape modelling and animation [37]. Guo et al. presented a scalar-field-driven editing paradigm and a system for point-set surfaces that allowed users to manipulate and sculpt point-clouds intuitively and efficiently [38]. McDonnell and Qin proposed a new volumetric subdivision scheme for the interpolation of arbitrary hexahedral meshes [39]. Huan and Qin presented a surface reconstruction algorithm that can recover correct shape geometry and its unknown topology from both volumetric images and unorganised point-clouds [40]. In order to maximise the modelling potential of PDE-based methodology, Du and Qin coupled PDEs with volumetric implicit functions achieving both intuitive and interactive shape representation, manipulation and deformation [41].

In this paper, we introduce a more general fourth order PDE for solid modelling. Whiles the technique presented in [31] can only deal with boundary positional continuity and give closed form solutions to some specific cases, our technique can also cope with boundary tangential continuity and has more vector-valued parameters. Thus, our technique provides better control over the shape of the generated PDE solid. In addition, our technique is able to consider a range of general cases of boundary conditions and present a unified closed form solution to our fourth order PDE. Compared to the numerical algorithm for solving the PDE used by Du and Qin [34], our closed form solution is much more efficient.

II. A Static PDE and its Closed Form Solution

First, let us introduce the formulation that we use to describe a PDE solid volume. This formulation is similar to the one used in our previous work to represent the surface model of objects [24].

Allowing for the effect of the boundary tangent on the shape of the solid volume, a PDE solid model can be generated from the solution of a fourth order PDE, shown in equation (1), which involves three parametric variables and is subject to the boundary conditions, given in equation (2).

$$\mathbf{a}\frac{\partial^4 \mathbf{x}}{\partial u^4} + \mathbf{b}\frac{\partial^4 \mathbf{x}}{\partial v^4} + \mathbf{c}\frac{\partial^4 \mathbf{x}}{\partial w^4} = \mathbf{p}(u,v,w) \tag{1}$$

$$\begin{aligned} w = 0 \qquad & \mathbf{x} = \mathbf{G}_1(u,v) \qquad \frac{\partial \mathbf{x}}{\partial w} = \overline{\mathbf{G}}_1(u,v) \\ w = 1 \qquad & \mathbf{x} = \mathbf{G}_2(u,v) \qquad \frac{\partial \mathbf{x}}{\partial w} = \overline{\mathbf{G}}_2(u,v) \end{aligned} \tag{2}$$

where $\mathbf{a}=[a_x\ a_y\ a_z]^T$, $\mathbf{b}=[b_x\ b_y\ b_z]^T$ and $\mathbf{c}=[c_x\ c_y\ c_z]^T$ are the vector-valued shape parameters of the PDE, $\mathbf{x}(u,\ v,\ w)=[x(u,\ v,\ w)\ y(u,\ v,\ w)\ z(u,\ v,\ w)]^T$ is a vector-valued positional function, $\mathbf{G}_1(u,v)$ and $\mathbf{G}_2(u,v)$ are the vector-valued functions of the boundary surfaces of the generated solid volume, $\overline{\mathbf{G}}_1(u,v)$ and $\overline{\mathbf{G}}_2(u,v)$ are the vector-valued functions of the boundary tangents of this volume, and $\mathbf{p}(u,v,w)$ is a vector-valued force function. All the vector-valued functions have three components x, y and z.

The PDE (1) subject to the boundary conditions (2) can be solved using the finite element method, the finite difference method or the weighted residual method. All these methods are effective in solving PDEs, but they are slow and far from ideal for interactive geometric modelling. To overcome this difficulty, we will develop an accurate and efficient closed form resolution method for our PDE.

The general solution of PDE (1) subject to boundary conditions (2) consists of a complementary solution of the associated homogeneous equation of the PDE and a particular solution of the non-homogeneous PDE.

In order to find the closed form complementary solution of PDE (1) subject to the boundary conditions (2), first we decompose the functions of the boundary conditions into some basic functions $\mathbf{g}_j(u,v)$ of a non-polynomial form (since each term of a polynomial is a basic function and a polynomial is the sum of a number of such basic functions). With these basic functions, we rewrite the boundary conditions (2) in the following form:

$$\begin{aligned} &w=0 \qquad \mathbf{x}=\sum_{j=1}^{J}\mathbf{a}_{1j}\mathbf{g}_j(u,v) \qquad \frac{\partial\mathbf{x}}{\partial w}=\sum_{j=1}^{J}\mathbf{a}_{2j}\mathbf{g}_j(u,v)\\ &w=1 \qquad \mathbf{x}=\sum_{j=1}^{J}\mathbf{a}_{3j}\mathbf{g}_j(u,v) \qquad \frac{\partial\mathbf{x}}{\partial w}=\sum_{j=1}^{J}\mathbf{a}_{4j}\mathbf{g}_j(u,v)\end{aligned} \tag{3}$$

Then, we construct a complementary solution of the associated homogeneous equation of PDE (1) which consists of the unknown functions of parametric variable w and the known basic boundary functions $\mathbf{g}_j(u,v)$, i. e.,

$$\mathbf{x}=\sum_{j=1}^{J}\mathbf{h}_j(w)\mathbf{g}_j(u,v) \tag{4}$$

Substituting equation (4) into PDE (1) while ignoring the force function, we obtain the following fourth order partial differential equation:

$$\mathbf{a}\mathbf{h}_j(w)\frac{\partial^4\mathbf{g}_j(u,v)}{\partial u^4}+\mathbf{b}\mathbf{h}_j(w)\frac{\partial^4\mathbf{g}_j(u,v)}{\partial v^4}+\mathbf{c}\mathbf{g}_j(u,v)\frac{\partial^4\mathbf{h}_j(w)}{\partial w^4}=0 \qquad (j=1,2,\cdots,J) \tag{5}$$

For the basic boundary functions whose fourth partial derivatives can be expressed with the basic boundary functions themselves, i.e.,

$$\begin{aligned}\frac{\partial^4\mathbf{g}_j(u,v)}{\partial u^4}&=\mathbf{b}_{u4j}\mathbf{g}_j(u,v)\\ \frac{\partial^4\mathbf{g}_j(u,v)}{\partial v^4}&=\mathbf{b}_{v4j}\mathbf{g}_j(u,v)\end{aligned} \tag{6}$$

equation (5) can be formulated below:

$$\frac{d^4\mathbf{h}_j(w)}{dw^4}-\mathbf{e}_j\mathbf{h}_j(w)=0 \qquad (j=1,2\cdots,J) \tag{7}$$

where $\mathbf{e}_j$ is a vector-valued constant that is given as:

$$\mathbf{e}_j=-\frac{\mathbf{a}\mathbf{b}_{u4j}+\mathbf{b}\mathbf{b}_{v4j}}{\mathbf{c}} \tag{8}$$

For the basic boundary functions whose fourth partial derivatives cannot be expressed with the basic boundary functions themselves, we can always transform them into those satisfying Eq. (6), e.g., a Fourier series.

Let us now consider the following two situations: $\mathbf{e}_j=0$ and $\mathbf{e}_j\neq 0$. If $\mathbf{e}_j=0$, equation (7) reduces to:

$$\frac{d^4\mathbf{h}_j(w)}{dw^4}=0 \qquad (j=1,2\cdots,J) \tag{9}$$

The solution to the above fourth order ordinary differential equations can be written as:

$$h_{tj}(w)=c_{t1}+c_{t2}w+c_{t3}w^2+c_{t4}w^3 \qquad (t=x,\ y,\ z;\ \ j=1,\ 2,\cdots,\ J) \tag{10}$$

where c_{t1}, c_{t2}, c_{t3} and c_{t4} are unknown constants, and $h_{xj}(w)$, $h_{yj}(w)$ and $h_{zj}(w)$ are the components of the vector-valued function $\mathbf{h}_j(w)$.

Substituting equation (9) into (4), the position function of the volume takes the form:

$$t=\sum_{j=1}^{J}\left(c_{t1}+c_{t2}w+c_{t3}w^2+c_{t4}w^3\right)g_{tj}(u,v) \qquad (t=x,\ y,\ z) \tag{11}$$

where $g_{xj}(u,v)$, $g_{yj}(u,v)$ and $g_{zj}(u,v)$ are the components of the vector-valued function $\mathbf{g}_j(u,v)$.

If $\mathbf{e}_j\neq 0$, the components of the unknown function $\mathbf{h}_j(w)$ can be taken to be:

$$h_{tj}(w)=e^{rw} \qquad (t=x,\ y,\ z) \tag{12}$$

Substituting equation (12) into (7), we obtain the following non-linear algebraic equations:

$$r^4-e_{tj}=0 \qquad (t=x,\ y,\ z;\ j=1,2,\cdots,J) \tag{13}$$

where e_{xj}, e_{yj} and e_{zj} are the components of the vector-valued constant $\mathbf{e}_j$.

Equation (13) is an algebraic equation. The solution of which consists of four roots that can be written as:

$$\begin{aligned}r_{t1,2}&=\pm\sqrt[4]{e_{tj}}\\ r_{t3,4}&=\pm i\sqrt[4]{e_{tj}}\end{aligned} \tag{14}$$

where i is the imaginary unit.

Using equation (14), we can rewrite the components of the unknown function $\mathbf{h}_j(w)$ as:

$$h_{tj}(w) = c_{t1}e^{\sqrt[4]{e_{tj}}w} + c_{t2}e^{-\sqrt[4]{e_{tj}}w} + c_{t3}\cos\sqrt[4]{e_{tj}}w + c_{t4}\sin\sqrt[4]{e_{tj}}w \quad (15)$$
$$(t = x, y, z;\ j = 1, 2, \cdots, J)$$

Substituting equation (15) into (4), the position function of the solid defined by the boundary conditions (3) becomes:

$$t = \sum_{j=1}^{J}\left[c_{t1}e^{\sqrt[4]{e_{tj}}w} + c_{t2}e^{-\sqrt[4]{e_{tj}}w} + c_{t3}\cos\sqrt[4]{e_{tj}}w + c_{t4}\sin\sqrt[4]{e_{tj}}w\right]g_{tj}(u,v) \quad (16)$$
$$(t = x, y, z)$$

Subject to the specified boundary conditions, the coefficient e_{tj} and the unknown constants c_{t1}, c_{t2}, c_{t3} and c_{t4} can be determined by substituting equations (11) or (16) into these boundary conditions.

From the theory of partial differential equations, we know that the particular solution of PDE (1) depends on the mathematical representation of the force function. Therefore, in the next section, we introduce a number of examples that show how we determine the particular solution of PDE (1).

Superimposing the particular solution on the complementary solution (11) or (16), we obtain the general solution of PDE (1) that can be used to generate the required solid volume.

III. The Generation of Solid Volumes

In this section, we discuss the application of the above-developed closed form solution to the modelling of a solid using a number of examples.

In our first example, we generate a solid volume defined by two planar surfaces whose boundary curves are square or rectangular. This example was selected to show how the geometric parameters of the boundary conditions affect the shape of generated PDE solid.

Here, the boundary conditions of the solid are given by:

$$\begin{array}{lll}
w=0 & x = a_0 + a_1 u & \dfrac{\partial x}{\partial w} = a_0' + a_1' u \\
 & y = b_0 + b_1 v & \dfrac{\partial y}{\partial w} = b_0' + b_1' v \\
 & z = h_0 & \dfrac{\partial z}{\partial w} = h_0' \\
w=1 & x = a_2 + a_3 u & \dfrac{\partial x}{\partial w} = a_2' + a_3' u \\
 & y = b_2 + b_3 v & \dfrac{\partial y}{\partial w} = b_2' + b_3' v \\
 & z = h_1 & \dfrac{\partial z}{\partial w} = h_1'
\end{array} \quad (17)$$

where a_i and b_i $(i = 0, 1, 2, 3)$ determine the shape and size of the planar boundary surfaces, h_0 and h_1 determine the relative height of these surfaces in the z direction, a_i', b_i' $(i = 0, 1, 2, 3)$, and h_0' and h_1' determine the direction and size of the tangents of the solid to be generated at the boundary surfaces.

The basic functions in the boundary conditions (17) are taken to be $g_{x1}(u,v) = 1$ and $g_{x2}(u,v) = u$ for the x component, $g_{y1}(u,v) = 1$ and $g_{y2}(u,v) = v$ for the y component, and $g_{z1}(u,v) = 1$ for the z component. Since $\mathbf{e}_1$ and $\mathbf{e}_2$ are equal to zero, the position function of the solid volume (11) becomes:

$$\begin{aligned}
x &= c_{x1} + c_{x2}w + c_{x3}w^2 + c_{x4}w^3 + \left(c_{x5} + c_{x6}w + c_{x7}w^2 + c_{x8}w^3\right)u \\
y &= c_{y1} + c_{y2}w + c_{y3}w^2 + c_{y4}w^3 + \left(c_{y5} + c_{y6}w + c_{y7}w^2 + c_{y8}w^3\right)v \\
z &= c_{z1} + c_{z2}w + c_{z3}w^2 + c_{z4}w^3
\end{aligned} \quad (18)$$

Substituting equation (18) into the boundary conditions (17), we determine all the unknown constants. Initially, we set the geometric parameters to the following values: $a_0 = b_0 = a_2 = b_2 = -0.5$, $a_1 = b_1 = a_3 = b_3 = h_1 = 1$, and $h_0 = a_0' = a_1' = b_0' = b_1' = a_2' = a_3' = b_2' = b_3' = h_0' = h_1' = 0$, and we obtain the cuboid shown in figures 1a and 1b. Then, we alter the values of some of the geometric parameters to the following values: $a_2 = b_2 = -1$ and $a_3 = b_3 = h_1 = 2$. The generated solid now becomes the irregular hexahedron shown in figures 1c and 1d. Setting the geometric parameters to the values: $a_0 = -0.5$, $a_1 = 1.5$, $a_2 = b_0 = -1$, $a_3 = b_1 = 3$, $b_2 = -0.4$, $b_3 = 1$, $h_0 = 0$, $h_1 = 2$, and $a_0' = a_0$, $a_1' = a_1$, $a_2' = a_2$, $a_3' = a_3$, $b_0' = b_0$, $b_1' = b_1$, $b_2' = b_2$, $b_3' = b_3$, $h_0' = h_1$ and $h_1' = 2h_1$, we obtain the solid depicted in figures 1e and 1f. Finally, changing the boundary tangents to $a_0' = 2.5a_0$, $a_1' = 2.5a_1$, $a_2' = -2a_2$, $a_3' = -2a_3$, $b_0' = -2.5b_0$, $b_1' = -2.5b_1$, and $h_1' = h_1$, resulted in the solid depicted in figures 1g and 1h.

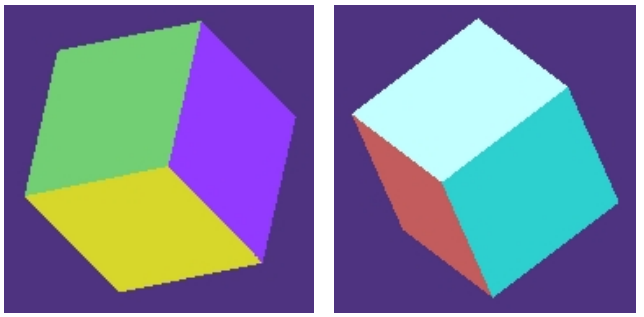

a b

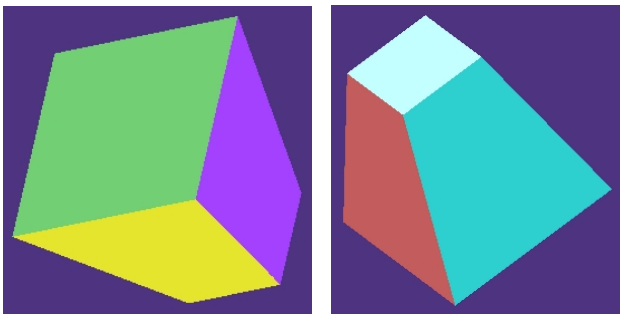

c d

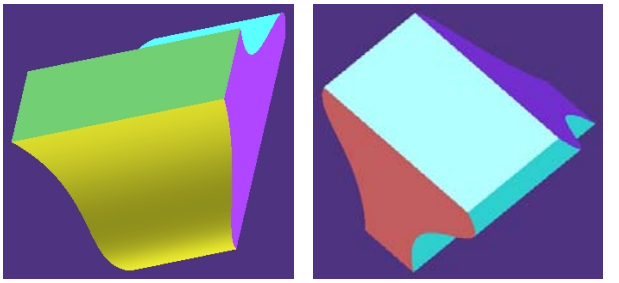

e f

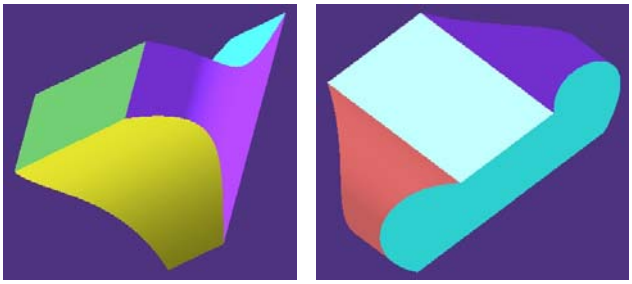

g h

Fig. 1 PDE solids defined by two parallel planar surfaces with square or rectangular boundary curves.

From figure 1, it is clear that varying the geometric parameters and tangents of the solid at the boundary surfaces can greatly affect the shape of the generated PDE solid.

Generating the images of the PDE solids presented in figure 1 was fairly straightforward. In each case, we did so by displaying the six isoparametric surfaces that represent the outer skin of the corresponding PDE solid. Using equation (18), we generated these isoparametric surfaces by keeping the value of one of the parametric variables (u,v,w) constant, while varying the values of the other two in the range $[0,1]$. Thus, for the first isoparametric surface we used $u=0$ and $v,w\in[0,1]$, for the second isoparametric surface $u=1$ and $v,w\in[0,1]$, and so on.

The second example is to generate a solid volume confined by one circle plane and one elliptic plane. This example is employed to demonstrate how the vector-valued parameters in Eq. (1) influence the shape of solids. The boundary conditions at the boundary surfaces have the following forms

$$\begin{aligned}
w=0 \quad & x=r_0 u\sin 2\pi v && \frac{\partial x}{\partial w}=r_0' u\sin 2\pi v\\
& y=r_0 u\cos 2\pi v && \frac{\partial y}{\partial w}=r_0' u\cos 2\pi v\\
& z=h_0 && \frac{\partial z}{\partial w}=h_0'\\
w=1 \quad & x=a_0 u\sin 2\pi v && \frac{\partial x}{\partial w}=a_0' u\sin 2\pi v\\
& y=b_0 u\cos 2\pi v && \frac{\partial y}{\partial w}=b_0' u\cos 2\pi v\\
& z=h_1 && \frac{\partial z}{\partial w}=h_1'
\end{aligned} \tag{19}$$

where r_0 and h_0 determine the size of the circle plane, r_0' and h_0' determine the direction and size of the tangent of the solid at the boundary plane, a_0, b_0 and h_1 determine the size of the elliptic plane, and a_0', b_0' and h_1' determine the direction and size of the tangent of the solid at the boundary elliptic plane.

The basic function in the above boundary conditions is $g_{x1}(u,v)=u\sin 2\pi v$ for the x component, $g_{y1}(u,v)=u\cos 2\pi v$ for the y component, and $g_{z1}(u,v)=1$ for the z component. The position functions (11) and (15) of the solid volume becomes

$$\begin{aligned}
x &= \left(c_{x1}e^{t_x w}+c_{x2}e^{-t_x w}+c_{x3}\cos t_x w+c_{x4}\sin t_x w\right)u\sin 2\pi v\\
y &= \left(c_{y1}e^{t_y w}+c_{y2}e^{-t_y w}+c_{y3}\cos t_y w+c_{y4}\sin t_y w\right)u\cos 2\pi v\\
z &= c_{z1}+c_{z2}w+c_{z3}w^2+c_{z4}w^3
\end{aligned} \tag{20}$$

where

$$t_i=2\pi\sqrt{-\frac{b_i}{c_i}} \qquad (i=x,y) \tag{21}$$

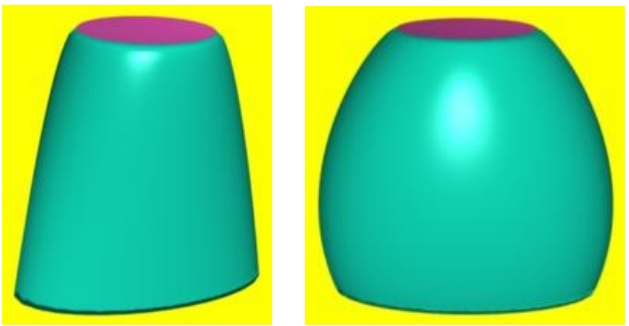

a b

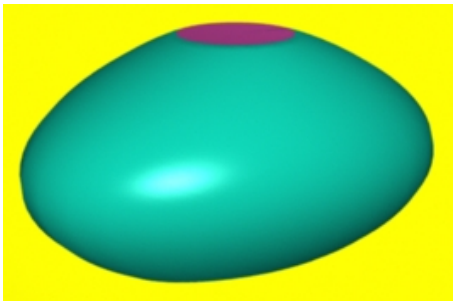

c

Fig. 2 Solids defined by two parallel planes confined by a circle and an ellipse

Substituting Eq. (20) into (19), all the unknown constants in Eq. (20) were determined. For this example, we examine how the vector-valued parameters affect the shape of the solid. Therefore, all the geometric parameters were fixed at $r_0=r_0'=a_0=0.5$, $b_0=1$, $h_0=h_0'=h_1'=a_0'=b_0'=0$, and $h_1=2$. Since the z component of the vector-valued parameters does not affect the solution function, we only consider the x and y components. Firstly, taking $a_x=a_y=1$, $b_x=b_y=4$ and $c_x=c_y=-100$, the image in Fig. 2a was obtained. Then, changing $c_x=c_y=-100$ to $c_x=c_y=-10$ and $b_x=b_y=4$ to $b_x=b_y=2.5$, the image was changed to that in Fig. 2b.

Finally, fixing $c_x = c_y = -10$ but changing $b_x = b_y = 2.5$ back to $b_x = b_y = 4$, the image in Fig. 2c was created. From these images, it is clear that the variety of the vector-valued has greatly changed the shape of the solid.

In our third example, we generate a solid volume defined by two planar or 3D boundary surfaces. This example was selected to show how different basic functions affect the shape of the generated PDE solids.

Here, the boundary conditions of the solid are given by:

$$\begin{array}{lll} w=0 & x = u(r_0 \sin 2\pi v + r_1 \sin n_{xy}\pi v) & \frac{\partial x}{\partial w} = u(r_0' \sin 2\pi v + r_1' \sin n_{xy}\pi v) \\ & y = u(r_0 \cos 2\pi v + r_1 \cos n_{xy}\pi v) & \frac{\partial y}{\partial w} = u(r_0' \cos 2\pi v + r_1' \cos n_{xy}\pi v) \\ & z = h_0 + h_1 u \sin n_z \pi v & \frac{\partial z}{\partial w} = h_0' + h_1' u \sin n_z \pi v \\ w=1 & x = r_2 u \sin 2\pi v & \frac{\partial x}{\partial w} = r_2' u \sin 2\pi v \\ & y = r_2 u \cos 2\pi v & \frac{\partial y}{\partial w} = r_2' u \cos 2\pi v \\ & z = h_2 + h_3 u \sin n_z \pi v & \frac{\partial z}{\partial w} = h_2' + h_3' u \sin n_z \pi v \end{array} \quad (22)$$

where r_0, r_1, h_0 and h_1 are geometric parameters determining the size of the top boundary surface, r_0', r_1', h_0' and h_1' determine the direction and size of the tangent of the solid at the top boundary surface, r_2, h_2 and h_3 are the geometric parameters determining the size of the bottom boundary surface, and r_2', h_2' and h_3' determine the direction and size of the tangent of the solid at the bottom boundary surface.

When n_z in equation (22) is set to 0, two planar boundary surfaces are described, otherwise two three-dimensional boundary surfaces are described.

The basic functions in the above boundary conditions are taken to be $g_{x1}(u,v) = u \sin 2\pi v$ and $g_{x2}(u,v) = u \sin n_{xy}\pi v$ for the x component, $g_{y1}(u,v) = u \cos 2\pi v$ and $g_{y2}(u,v) = u \cos n_{xy}\pi v$ for the y component, and $g_{z1}(u,v) = 1$ and $g_{z2}(u,v) = u \sin n_z \pi v$ for the z component. The solution functions are:

$$\begin{aligned} x &= \left(c_{x11}e^{t_{x1}w} + c_{x21}e^{-t_{x1}w} + c_{x31}\cos t_{x1}w + c_{x41}\sin t_{x1}w\right)u \sin 2\pi v \\ &\quad + \left(c_{x12}e^{t_{x2}w} + c_{x22}e^{-t_{x2}w} + c_{x32}\cos t_{x2}w + c_{x42}\sin t_{x2}w\right)u \sin n_{xy}\pi v \\ y &= \left(c_{y11}e^{t_{y1}w} + c_{y21}e^{-t_{y1}w} + c_{y31}\cos t_{y1}w + c_{y41}\sin t_{y1}w\right)u \cos 2\pi v \\ &\quad + \left(c_{y12}e^{t_{y2}w} + c_{y22}e^{-t_{y2}w} + c_{y32}\cos t_{y2}w + c_{y42}\sin t_{y2}w\right)u \cos n_{xy}\pi v \\ z &= c_{z11} + c_{z21}w + c_{z31}w^2 + c_{z41}w^3 + (c_{z12}e^{t_z w} + c_{z22}e^{-t_z w} + c_{z32}\cos t_z w \\ &\quad + c_{z42}\sin t_z w)u \sin n_z \pi v \end{aligned} \quad (23)$$

where

$$\begin{aligned} t_{i1} &= 2\pi\sqrt{-\frac{b_i}{c_i}} \\ t_{i2} &= n_{xy}\pi\sqrt{-\frac{b_i}{c_i}} \\ (i &= x, y) \\ t_z &= n_z\pi\sqrt{-\frac{b_z}{c_z}} \end{aligned} \quad (24)$$

In this example, the vector-valued parameters were set to $a_x = a_y = a_z = 1$, $b_x = b_y = b_z = 2.5$ and $c_x = c_y = c_z = -10$, and the geometric parameters were set to $r_0 = 0.5$, $r_1 = h_1 = 0.1$, $r_2 = 0.5$, $h_0 = 2$, $h_2 = 0$, $h_3 = -0.1$, and $r_0' = r_1' = r_2' = h_0' = h_1' = h_2' = h_3' = 0$. The solid depicted in figure 3a was generated by setting $n_{xy} = 20$ and $n_z = 0$. Changing n_{xy} to 30, generated the solid depicted in figure 3b. Setting $r_2 = 0.8$, $n_{xy} = 8$ and $n_z = 10$, resulted in the solid depicted in figure 3c. Finally, setting $n_{xy} = 14$ and $n_z = 6$, resulted in the solid depicted in figure 3d.

Examining these images we can conclude that selecting different basic functions (i.e. $u \sin 20\pi v$, $u \sin 30\pi v$, $u \sin 8\pi v$ and $u \sin 14\pi v$ for the x component, $u \cos 20\pi v$, $u \cos 30\pi v$, $u \cos 8\pi v$ and $u \cos 14\pi v$ for the y component, and $u \sin 10\pi v$ and $u \sin 6\pi v$ for the z component) greatly influences the shape of the generated solid.

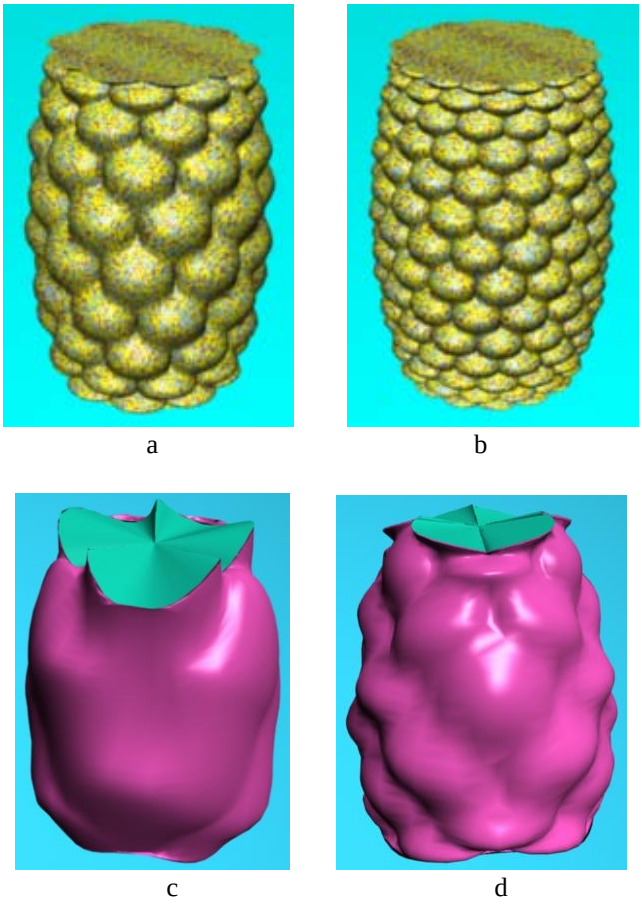

a b c d

Fig. 3 PDE solids defined by two planar or three-dimensional surfaces.

In our fourth example, we generate a solid volume defined by two boundary surfaces confined within two circles and subjected to a vector-valued force function. This example was selected to show how different combinations of the vector-valued parameters, force function, boundary positions and tangents have the capacity to generate solids with widely diverse shapes.

Here, the boundary conditions of the solid are given by:

$$
\begin{array}{lll}
w=0 & x=r_0 u\sin 2\pi v & \dfrac{\partial x}{\partial w}=r_0' u\sin 2\pi v \\
 & y=r_0 u\cos 2\pi v & \dfrac{\partial y}{\partial w}=r_0' u\cos 2\pi v \\
 & z=h_0 & \dfrac{\partial z}{\partial w}=h_0' \\
w=1 & x=r_1 u\sin 2\pi v & \dfrac{\partial x}{\partial w}=r_1' u\sin 2\pi v \\
 & y=r_1 u\cos 2\pi v & \dfrac{\partial y}{\partial w}=r_1' u\cos 2\pi v \\
 & z=h_1 & \dfrac{\partial z}{\partial w}=h_1'
\end{array} \tag{25}
$$

where r_0 and h_0 determine the size of the upper boundary surface, r_0' and h_0' determine the direction and size of the tangent of the solid at this boundary, r_1 and h_1 determine the size of the bottom boundary surface, and r_1' and h_1' determine the direction and size of the tangent of the solid at this boundary.

The basic functions in the above boundary conditions are given by $g_{x1}(u,v)=u\sin 2\pi v$ for the x component, $g_{y1}(u,v)=u\cos 2\pi v$ for the y component, and $g_{z1}(u,v)=1$ for the z component. Now, the position functions (11) and (16) of the solid volume become:

$$
\begin{aligned}
\bar{x} &= \left(c_{x1}e^{t_x w}+c_{x2}e^{-t_x w}+c_{x3}\cos t_x w+c_{x4}\sin t_x w\right)u\sin 2\pi v \\
\bar{y} &= \left(c_{y1}e^{t_y w}+c_{y2}e^{-t_y w}+c_{y3}\cos t_y w+c_{y4}\sin t_y w\right)u\cos 2\pi v \\
\bar{z} &= c_{z1}+c_{z2}w+c_{z3}w^2+c_{z4}w^3
\end{aligned} \tag{26}
$$

where

$$
t_i = 2\pi\sqrt{-\frac{b_i}{c_i}} \qquad (i=x,\,y) \tag{27}
$$

As we now wish to consider the effect of the force function on the shape of the generated solid, we represent this function in the following form:

$$
\begin{aligned}
p_x(u,v,w) &= p_0 u\sin\xi\pi w\cos 2\pi v \\
p_y(u,v,w) &= p_0 u\sin\xi\pi w\sin 2\pi v \\
p_z(u,v,w) &= 0
\end{aligned} \tag{28}
$$

Substituting equation (28) into PDE (1), the particular solution of the non-homogeneous fourth order PDE is given as:

$$
\begin{aligned}
\bar{\bar{x}} &= \frac{p_0}{(16b_x+c_x\xi^4)\pi^4}u\sin\xi\pi w\cos 2\pi v \\
\bar{\bar{y}} &= \frac{p_0}{(16b_y+c_y\xi^4)\pi^4}u\sin\xi\pi w\sin 2\pi v \\
\bar{\bar{z}} &= 0
\end{aligned} \tag{29}
$$

Superimposition of equation (29) onto equation (26) results in the general solution of the non-homogeneous fourth order PDE (1), which has the form:

$$
\begin{aligned}
x &= \left(c_{x1}e^{t_x w}+c_{x2}e^{-t_x w}+c_{x3}\cos t_x w+c_{x4}\sin t_x w\right)u\sin 2\pi v \\
&\quad+\frac{p_0}{(16b_x+c_x\xi^4)\pi^4}u\sin\xi\pi w\cos 2\pi v \\
y &= \left(c_{y1}e^{t_y w}+c_{y2}e^{-t_y w}+c_{y3}\cos t_y w+c_{y4}\sin t_y w\right)u\cos 2\pi v \\
&\quad+\frac{p_0}{(16b_y+c_y\xi^4)\pi^4}u\sin\xi\pi w\sin 2\pi v \\
z &= c_{z1}+c_{z2}w+c_{z3}w^2+c_{z4}w^3
\end{aligned} \tag{30}
$$

Substituting equation (30) into (25), we determine all the unknown constants in equation (30) and use it to generate the solid.

Different combinations of the vector-valued parameters, force function, and positional and tangential parameters are listed below and the corresponding solids they generate are shown in figure 4.

Fig. 4a: $b_x=b_y=1$, $c_x=c_y=-9.5$, $r_0=0.5$, $r_0'=0$, $r_1=0.5$, $r_1'=0$, $h_0=0$, $h_0'=0$, $h_1=3$, $h_1'=7.5$, $p_0=3\times10^4$ and $\xi=3$.

Fig. 4b: $b_x=b_y=2.5$, $c_x=c_y=-10$, $r_0=0.5$, $r_0'=2.5$, $r_1=0.5$, $r_1'=2.5$, $h_0=0$, $h_0'=0$, $h_1=3$, $h_1'=3$, $p_0=8\times10^4$ and $\xi=5$.

Fig. 4c: $b_x=b_y=4$, $c_x=c_y=-100$, $r_0=0.5$, $r_0'=2.5$, $r_1=0.5$, $r_1'=2.5$, $h_0=0$, $h_0'=0$, $h_1=3$, $h_1'=6$, $p_0=1.8\times10^6$ and $\xi=7$.

Fig. 4d: $b_x=b_y=4$, $c_x=c_y=-10$, $r_0=0.5$, $r_0'=-1.5$, $r_1=0.5$, $r_1'=2$, $h_0=0$, $h_0'=3$, $h_1=3$, $h_1'=6$, $p_0=3\times10^5$ and $\xi=7$.

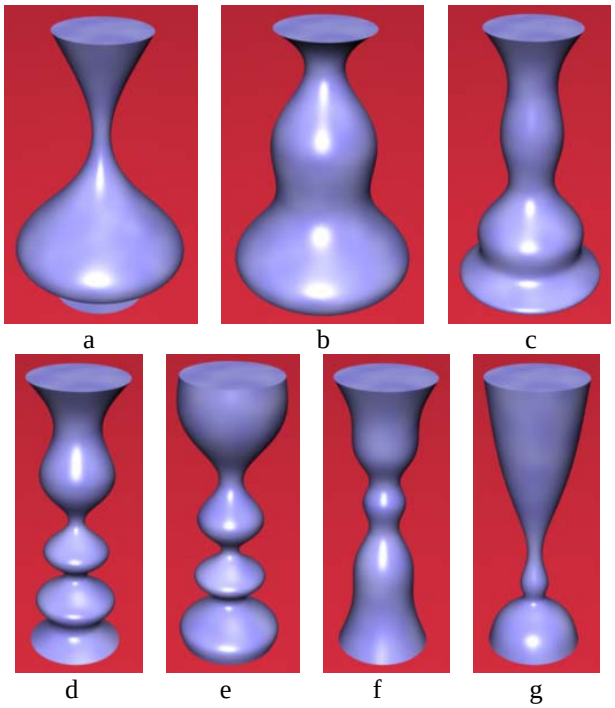

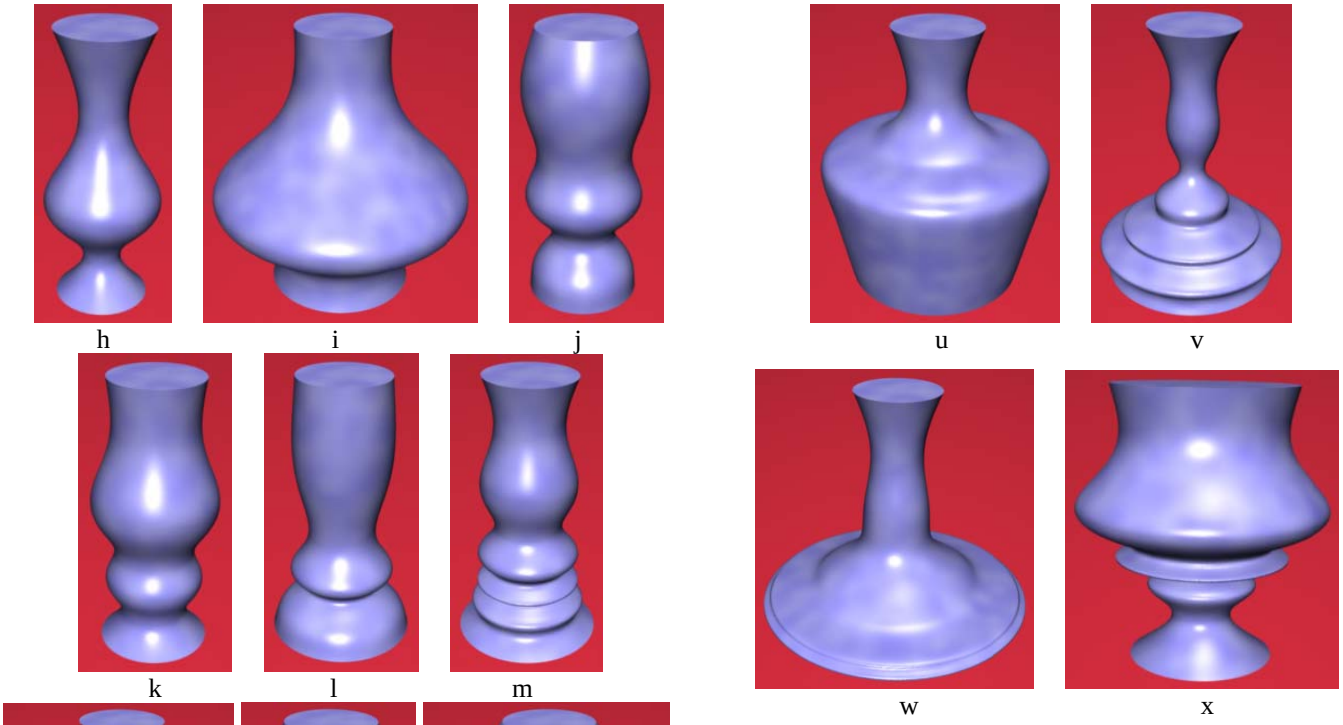

Fig. 4 Solids generated using different combinations of the parameters controlling their shape.

Fig. 4e: $b_x = b_y = 4$, $c_x = c_y = -10$, $r_0 = 0.5$, $r_0' = -1.5$, $r_1 = 0.5$, $r_1' = 2$, $h_0 = 0$, $h_0' = 3$, $h_1 = 3$, $h_1' = 6$, $p_0 = -3\times10^5$ and $\xi = 7$.

Fig. 4f: $b_x = b_y = 2.5$, $c_x = c_y = -10$, $r_0 = 0.5$, $r_0' = -1.5$, $r_1 = 0.5$, $r_1' = 1.5$, $h_0 = 0$, $h_0' = 6$, $h_1 = 3$, $h_1' = 4.5$, $p_0 = 10^5$ and $\xi = 7$.

Fig. 4g: $b_x = b_y = 2.5$, $c_x = c_y = -10$, $r_0 = 0.5$, $r_0' = -1.5$, $r_1 = 0.5$, $r_1' = 2$, $h_0 = 0$, $h_0' = 3$, $h_1 = 3$, $h_1' = 9$, $p_0 = -3\times10^4$ and $\xi = 5$.

Fig. 4h: $b_x = b_y = 2.5$, $c_x = c_y = -10$, $r_0 = 0.5$, $r_0' = -1$, $r_1 = 0.5$, $r_1' = 0.5$, $h_0 = 0$, $h_0' = 3$, $h_1 = 3$, $h_1' = 6$, $p_0 = 1.5\times10^4$ and $\xi = 3$.

Fig. 4i: $b_x = b_y = 2.5$, $c_x = c_y = -10$, $r_0 = 0.8$, $r_0' = 0.8$, $r_1 = 0.5$, $r_1' = -1.6$, $h_0 = 0$, $h_0' = 3$, $h_1 = 3$, $h_1' = 6$, $p_0 = 1.5\times10^4$ and $\xi = 3$.

Fig. 4j: $b_x = b_y = 2.5$, $c_x = c_y = -10$, $r_0 = 0.6$, $r_0' = -1.8$, $r_1 = 0.5$, $r_1' = -0.6$, $h_0 = 0$, $h_0' = 3$, $h_1 = 3$, $h_1' = 6$, $p_0 = -5.5\times10^4$ and $\xi = 5$.

Fig. 4k: $b_x = b_y = 2.5$, $c_x = c_y = -10$, $r_0 = 0.6$, $r_0' = -1.8$, $r_1 = 0.5$, $r_1' = -0.6$, $h_0 = 0$, $h_0' = 3$, $h_1 = 3$, $h_1' = 6$, $p_0 = 5.5\times10^4$ and $\xi = 5$.

Fig. 4l: $b_x = b_y = 3.5$, $c_x = c_y = -10$, $r_0 = 0.8$, $r_0' = -2.4$, $r_1 = 0.5$, $r_1' = 0.5$, $h_0 = 0$, $h_0' = 3$, $h_1 = 3$, $h_1' = 9$, $p_0 = -5.5\times10^4$ and $\xi = 5$.

Fig. 4m: $b_x = b_y = 3.5$, $c_x = c_y = -10$, $r_0 = 0.8$, $r_0' = -2.4$, $r_1 = 0.5$, $r_1' = 0.5$, $h_0 = 0$, $h_0' = 3$, $h_1 = 3$, $h_1' = 9$, $p_0 = 5.5\times10^4$ and $\xi = 9$.

Fig. 4n: $b_x = b_y = 5$, $c_x = c_y = -20$, $r_0 = 1.5$, $r_0' = -4.5$, $r_1 = 0.5$, $r_1' = 0$, $h_0 = 0$, $h_0' = 3$, $h_1 = 3$, $h_1' = 3$, $p_0 = 5\times10^5$ and $\xi = 7$.

Fig. 4o: $b_x = b_y = 3$, $c_x = c_y = -20$, $r_0 = 1$, $r_0' = -5$, $r_1 = 0.5$, $r_1' = -1$, $h_0 = 0$, $h_0' = 6$, $h_1 = 3$, $h_1' = 6$, $p_0 = -9\times10^5$ and $\xi = 11$.

Fig. 4p: $b_x = b_y = 15$, $c_x = c_y = -40$, $r_0 = 1$, $r_0' = -2$, $r_1 = 0.5$, $r_1' = -1$, $h_0 = 0$, $h_0' = 6$, $h_1 = 3$, $h_1' = 4.5$, $p_0 = 3\times10^6$ and $\xi = 11$.

Fig. 4q: $b_x = b_y = 1$, $c_x = c_y = -10$, $r_0 = 1$, $r_0' = 3$, $r_1 = 0.5$, $r_1' = -1$, $h_0 = 0$, $h_0' = 6$, $h_1 = 3$, $h_1' = 9$, $p_0 = 3\times10^4$ and $\xi = 3$.

Fig. 4r: $b_x = b_y = 1$, $c_x = c_y = -10$, $r_0 = 1$, $r_0' = -3$, $r_1 = 0.5$, $r_1' = -2$, $h_0 = 0$, $h_0' = 9$, $h_1 = 3$, $h_1' = 3$, $p_0 = 3\times10^4$ and $\xi = 3$.

Fig. 4s: $b_x = b_y = 1$, $c_x = c_y = -10$, $r_0 = 1$, $r_0' = -3$, $r_1 = 0.5$, $r_1' = -2$, $h_0 = 0$, $h_0' = 9$, $h_1 = 3$, $h_1' = 3$, $p_0 = 3\times10^5$ and $\xi = 7$.

Fig. 4t: $b_x = b_y = 1$, $c_x = c_y = -10$, $r_0 = 1$, $r_0' = -3$, $r_1 = 0.5$, $r_1' = -1$, $h_0 = 0$, $h_0' = 9$, $h_1 = 3$, $h_1' = 0$, $p_0 = 3\times10^5$ and $\xi = 5$.

Fig. 4u: $b_x = b_y = 1$, $c_x = c_y = -10$, $r_0 = 1$, $r_0' = 3$, $r_1 = 0.5$, $r_1' = 1$, $h_0 = 0$, $h_0' = 9$, $h_1 = 3$, $h_1' = 7.5$, $p_0 = 3\times10^4$ and $\xi = 5$.

Fig. 4v: $b_x = b_y = 1$, $c_x = c_y = -10$, $r_0 = 1$, $r_0' = 1$, $r_1 = 0.5$, $r_1' = 3$, $h_0 = 0$, $h_0' = 3$, $h_1 = 3$, $h_1' = 9$, $p_0 = 5\times10^5$ and $\xi = 9$.

Fig. 4w: $b_x = b_y = 1$, $c_x = c_y = -10$, $r_0 = 1$, $r_0' = 6$, $r_1 = 0.5$, $r_1' = 3$, $h_0 = 0$, $h_0' = 3$, $h_1 = 3$, $h_1' = 10.5$, $p_0 = 3\times10^5$ and $\xi = 9$.

Fig. 4x: $b_x = b_y = 1$, $c_x = c_y = -10$, $r_0 = 0.8$, $r_0' = -4$, $r_1 = 1$, $r_1' = -2.4$, $h_0 = 0$, $h_0' = 6$, $h_1 = 3$, $h_1' = 9$, $p_0 = 5\times10^5$ and $\xi = 7$.

From the images shown in this figure, it is clear that by combining different force functions and other parameters, a large variety of solid shapes can easily be generated.

IV. Conclusions

In this paper, a solid modelling method has been developed. It is based on our proposed fourth order partial differential equations and boundary conditions. By introducing the method of variable separation, the unified forms of the closed form solutions to the partial differential equations subjected to the boundary conditions are obtained.

With the obtained closed form solution, four examples have been given to demonstrate how solid models are represented and manipulated. We have also shown how different vector-valued parameters, force function, geometric parameters and basic functions affect the shape of the solids. Due to the analytical nature of the representations, the proposed method is accurate and has a high efficiency in solid modeling.

References

[1] H. Ugail and S. Kirmani, "Shape reconstruction using partial differential equations," *WSEAS Transactions on Computers*, vol. 5, pp. 2156-2161, 2006.

[2] S. F. Qin and D. Wright, "Universal attraction force-inspired freeform surface modelling for 3D sketching," *WSEAS Transactions on Computers*, vol. 5, pp. 1333-1338, 2006.

[3] G. Mo and Y. Zhao, "A new method for designing approximate developable surfaces," *WSEAS Transactions on Computers*, vol. 5, pp. 1130-1135, 2006.

[4] D. Terzopoulos, J. Platt, A. Barr and K. Fleischer, "Elastically deformable models," *Computer Graphics*, vol. 21, pp. 205-214, 1987.

[5] D. Terzopoulos and K. Fleischer, "Modelling inelastic deformation: viscoelasticity, plasticity, fracture," *Computer Graphics*, vol. 22, pp. 269-278, 1988.

[6] D. Terzopoulos and K. Fleischer, "Deformable models," *The Visual Computer*, vol. 4, pp. 306-331, 1988.

[7] D. Terzopoulos and H. Qin, "Dynamic NURBS with geometric constraints for interactive sculpting," *ACM Transactions on Graphics*, vol. 13, pp. 103-136, 1994.

[8] H. Qin and D. Terzopoulos, "Dynamic NURBS swung surfaces for physical-based shape design," *Computer-Aided Design*, vol. 27, pp. 111-127, 1995.

[9] H. Qin and D. Terzopoulos, "Triangular NURBS and their dynamic generations," *Computer Aided Geometric Design*, vol. 14, pp. 325-347, 1997.

[10] J. C. Léon and P. Veron, "Semiglobal deformation and correction of free-form surfaces using a mechanical alternative," *The Visual Computer*, vol. 13, pp. 109-126, 1997.

[11] S. Guillet and J. C. Léon, "Parametrically deformed free-form surfaces as part of a variational model," *Computer-Aided Design*, vol. 30, pp. 621-630, 1998.

[12] G. Celniker and D. Gossard, "Deformable curve and surface finite-elements for free-form shape design," *Computer Graphics*, vol. 25, pp. 257-266, 1991.

[13] H. Kang and A. Kak, "Deforming virtual objects interactively in accordance with an elastic model," *Computer-Aided Design*, vol. 28, pp. 251-262, 1996.

[14] T. I. Vassilev, "Interactive sculpting with deformable nonuniform B-splines," *Computer Graphics Forum*, vol. 16, pp. 191-199, 1997.

[15] M. I. G. Bloor and M. J. Wilson, "Generating blend surfaces using partial differential equations," *Computer Aided Design*, vol. 21, pp. 165-171, 1989.

[16] M. I. G. Bloor and M. J. Wilson, "Using partial differential equations to generate free-form surfaces," *Computer-Aided Design*, vol. 22, pp. 202-212, 1990.

[17] J. Monterde and H. Ugail, "On harmonic and biharmonic Bézier surfaces," *Computer Aided Geometric Design*, vol. 21, pp. 697-715, 2004.

[18] J. M. Brown, M. I. G. Bloor, M. S. Bloor and M. J. Wilson, "The accuracy of B-spline finite element approximations to PDE surfaces," *Computer methods in Applied Mechanics and Engineering*, vol. 158, pp. 221-234, 1998.

[19] Z. C. Li and C.-S. Chang, "Boundary penalty finite element methods for blending surfaces, III. Superconvergence and stability and examples," *Journal of Computational and Applied Mathematics*, vol. 110, pp. 241-270, 1999.

[20] C. Y. Cheng, M. I. G. Bloor, A. Saia and M. J. Wilson, "Blending between quadric surfaces using partial differential equations," in Ravani, B. (Ed.), *Advances in Design Automation*, vol. 1, Computer and Computational Design, ASME, pp. 257-263, 1990.

[21] M. I. G. Bloor and M. J. Wilson, "Representing PDE surfaces in terms of B-splines," *Computer-Aided Design*, vol. 22, pp. 324-331, 1990.

[22] M. I. G. Bloor and M. J. Wilson, "Spectral approximations to PDE surfaces," *Computer-Aided design*, vol. 28, pp.145-152, 1996.

[23] L. H. You and J. J. Zhang, "Blending surface generation with a fourth order partial differential equation," *The Sixth International Conference on Computer-Aided Design and Computer Graphics (CAD/Graphics'99)*, Shanghai, China, 1-5, December, 1999.

[24] L. H. You, J. J. Zhang and P. Comninos, "Blending surface generation using a fast and accurate analytical solution of a fourth order PDE with three shape control parameters," *The Visual Computer*, vol. 20, pp. 199-214, 2004.

[25] L. H. You, P. Comninos and J. J. Zhang, "PDE blending surfaces with c^2 continuity," *Computers & Graphics*, vol. 28, pp. 895-906, 2004.

[26] J. J. Zhang and L. H. You, "PDE based surface representation-Vase design," *Computers & Graphics*, vol. 26, pp. 89-98, 2002.

[27] J. J. Zhang and L. H. You, "Fast surface modelling using a 6th order PDE," *Computer Graphics Forum (Eurographics2004)*, vol. 23, pp. 311-320, 2004.

[28] A. H. Barr, "Global and local deformations of solid primitives," in *Proc. SIGGRAPH '84*, pp. 47-58, 1984.

[29] A. A. G. Requicha and J. R. Rossignac, "Solid modeling and beyond," *IEEE Computer Graphics and Applications*, vol. 12, pp. 31-44, 1992.

[30] D. Metaxas and D. Terzopoulos, "Dynamic deformation of solid primitives with constraints," *Computer Graphics (SIGGRAPH '92, Proc.)*, vol. 26, pp. 309-312, 1992.

[31] M. I. G. Bloor and M. J. Wilson, "Functionality in solids obtained from partial differential equations," *Computing Suppl*., vol. 8, pp. 21-42, 1993.

[32] E. Ferley, M. Cani and J. Gascuel, "Practical volumetric sculpting," *The Visual Computer*, vol. 16, pp. 469-480, 2000 .

[33] D. E. Breen and R. T. Whitaker, "A level-set approach for the metamorphosis of solid models," *IEEE Transactions on Visualization and Computer Graphics*, vol. 7, pp. 173-192, 2001.

[34] H. Du and H. Qin, "Integrating physics-based modelling with PDE solids for geometric design," in *Proceedings of Ninth Pacific Conference on Computer Graphics and Applications*, 16-18, October, Tokyo, Japan, published by IEEE Computer Society, pp. 198-207, 2001.

[35] K. T. McDonnell and H. Qin, "Dynamic sculpting and animation of free-form subdivision solids," *The Visual Computer*, vol. 18, pp. 81-96, 2002.

[36] J. Hua and H. Qin, "Haptics-based dynamic implicit solid modeling," *IEEE Transactions on Visualization and Computer Graphics*, vol. 10, pp. 574-586, 2004.

[37] J. Hua and H. Qin, "Scalar-field-guided adaptive shape deformation and animation," *The Visual Computer*, vol. 20, pp. 47-66, 2004.

[38] X. Guo, J. Hua and H. Qin, "Scalar-function-driven editing on point set surfaces," *IEEE Computer Graphics and Applications*, vol. 24, pp. 43-52, 2004.

[39] K. T. McDonnell and H. Qin, "Interpolatory, solid subdivision of unstructured hexahedral meshes," *The Visual Computer*, vol. 20, pp. 418-436, 2004.

[40] Y. Huan, and H. Qin, "A subdivision-based deformable model for surface reconstruction of unknown topology," *Graphical Models*, vol. 66, pp. 181-202, 2004.

[41] H. Du, and H. Qin, "A shape design system using volumetric implicit PDEs," *Computer-Aided Design*, vol. 36, pp. 1101-1116, 2004.